Global Dirac phenomenology for proton-nucleus elastic scattering

E. D. Cooper, S. Hama, and B. C. Clark
Department of Physics, The Ohio State University, Columbus, Ohio 43210

R. L. Mercer
IBM Thomas J. Watson Research Center, Yorktown Heights, New York 10598
(Received 31 August 1992)

Energy-dependent global Dirac optical model potentials are found by fitting proton elastic scattering data in the energy range 20–1040 MeV for ^{12}C, ^{16}O, ^{40}Ca, ^{90}Zr, and ^{208}Pb. Three different energy- and atomic-mass-number-dependent global Dirac optical potentials are also obtained. A number of characteristic features of the potentials are discussed. In addition, the mean free path, the effective mass m_e^*, the Dirac mass M^*, and the relativistic energy shift E^* are calculated.

PACS number(s): 24.10.Ht, 25.40.Cm

I. INTRODUCTION

For several years Dirac phenomenology has been used to determine global nucleon-nucleus optical potentials which span energies from 20 to 1040 MeV [1–3]. This phenomenology, which uses the Dirac equation to describe the dynamics of the nucleon, naturally admits the major characteristics of the nonrelativistic nuclear optical potential, namely, its central and spin-orbit terms. It easily accommodates the underlying nucleon and meson degrees of freedom which form the basis of descriptions of the nucleon-nucleon force at distances relevant to most nuclear phenomena. Moreover, the incorporation of relativistic dynamics is certainly warranted at medium energies. Recent work by Cohen, Furnstahl, and Griegel provides interesting evidence that the large scalar and vector fields of Dirac phenomenology may be related to quark degrees of freedom of the nucleon [4]. This work may lead to links between successful nuclear phenomenology employing large and canceling Lorentz scalar and vector fields and QCD.

The global potentials described in this paper give needed input for the analysis of a large number of nuclear reactions and provide a testing ground for more fundamental treatments of the nuclear optical model. To the best of our knowledge, the quality of the fits that we achieve and the energy and target mass range considered provide the most complete global optical model potential currently available. Results for heavy spin-zero targets and proton energies from 20 to 1040 MeV were presented in Refs. [1–3]. This paper is a continuation of that work in which the analysis is extended to light targets. In particular, we present energy-dependent but A-independent global potentials which reproduce proton scattering observables for proton energies from 20 to 1040 MeV for the following targets: ^{12}C, ^{16}O, ^{40}Ca, ^{90}Zr, and ^{208}Pb. In addition, we have found energy- and A-dependent global optical potentials for this energy region obtained by fitting proton elastic scattering observables from 10 spin-zero targets including those mentioned above.

In Sec. II the form of the global optical potential is presented. In Sec. III the data sets used in the analysis and their treatment are delineated. Section IV gives the results from the A-independent and A-dependent analyses. Section V gives a brief summary.

II. THE GLOBAL RELATIVISTIC OPTICAL MODEL POTENTIALS

This work uses the scalar-vector (SV) model of Dirac phenomenology, which has been successful in producing excellent agreement with elastic proton-nucleus scattering observables; see, for example, Refs. [1–3]. The general form of the scalar or vector optical model potentials is written

$$U(r,E,A)=V^V(E,A)f^V(r,E,A)+V^S(E,A)f^S(r,E,A) +iW^V(E,A)g^V(r,E,A) +iW^S(E,A)g^S(r,E,A)\ , \quad (1)$$

where the superscripts V and S refer to volume or surface peaked terms. Because we consider only proton data we did not include a term dependent on isospin. The global extraction of the isovector potential will be the subject of future work. Previously [3], no surface peaked term was present in the real part of the potential and the geometries were taken to be symmetrized Woods-Saxon (SWS) shapes

$$f^V \text{ and } g^V=\left[1+\exp\frac{[r-R(E,A)]}{a(E,A)}\right]^{-1} \times\left[1+\exp\frac{-[r+R(E,A)]}{a(E,A)}\right]^{-1}\ , \quad (2)$$

with the surface peaked geometries given by

$$g^S(r,E,A)=a^S(E,A)\frac{d}{dR}g^V(r,E,A)\ . \quad (3)$$

In this paper, we use a geometry that is similar to the SWS that we call the COSH form, in which the geometries are written

 ©1993 The American Physical Society

$$f^V \text{ and } g^V = \frac{\{\cosh[R(E,A)/a(E,A)]-1\}}{\{\cosh[R(E,A)/a(E,A)]+\cosh[r/a(E,A)]-2\}} , \tag{4}$$

$$f^S \text{ and } g^S = \frac{\{\cosh[R(E,A)/a(E,A)]-1\}\{\cosh[r/a(E,A)]-1\}}{\{\cosh[R(E,A)/a(E,A)]+\cosh[r/a(E,A)]-2\}^2} . \tag{5}$$

This form has several useful features when considering A-dependent fits. For example, for all A, $f^V(r=0)=1$, $f^V(r=R)=0.5$, $f^S(r=0)=0$, and $f^S(r=R)=0.25$. The SWS and COSH form factors have very similar shapes; however, the behavior of the COSH form at the origin and at $r=R$ is advantageous when using global potentials which are functions of target mass number as well as projectile energy. We found that the COSH form gave slightly better fits to the data than the SWS form.

The optical potential consists of scalar and vector terms each having real and imaginary parts. Each of the eight strengths, for example $V^V(E,A)$ in Eq. (1), is parametrized in terms of the proton c.m. energy E and A, the atomic mass number of the target. In this work we do not include any theoretical constraints on the parameters although we have done so in the past (see for example Ref. [1]). Instead we use, as we did in Ref. [3], polynomials of the form

$$V^V(E,A)=v_0+\sum_{m=1}^{4} v_m x^m+\sum_{n=1}^{3} v_{n+4} y^n+v_8 xy + v_9 x^2 y + v_{10} x y^2 , \tag{6}$$

where $x=1000/E$, $y=A/(A+20)$. The same form is used for the rest of the potentials $V^S(E,A)$, $W^V(E,A)$, and $W^S(E,A)$. The scalar and vector potentials and their real and imaginary parts all have different geometry parameters. The form of the E and A dependence is given by

$$R = A^{1/3}\left[r_0+\sum_{m=1}^{4} r_m x^m+\sum_{n=1}^{3} r_{n+4} y^n+r_8 xy + r_9 x^2 y + r_{10} x y^2\right] , \tag{7}$$

$$a=a_0+\sum_{m=1}^{4} a_m x^m+\sum_{n=1}^{3} a_{n+4} y^n+a_8 xy + a_9 x^2 y + a_{10} x y^2 . \tag{8}$$

This potential model has a maximum of 264 parameters although we have not used all of them. The generality of the parametrization allows us to accommodate both light and heavy targets and to extend the analysis to include energies between 65 and 20 MeV. We find that in order to obtain acceptable agreement with experiment more parameters are required than in our previous E- and A-dependent global analysis, which included only heavy targets and energies from 65 to 1040 MeV [3]. In the actual fitting procedure the geometrical parameters for the potentials are taken to be the same for surface and volume forms, reducing the number of parameters varied to 176. In order to allow tests of the sensitivity of the reaction under consideration to the input optical model potentials, two other global potentials were also found. In the first of these optical potentials the real surface peaked terms are set to zero reducing the number of parameters to 154; a further reduction to 106 terms is made by removing the A dependence in the imaginary surface potentials and by setting the cross terms in Eqs. (6)–(8) to zero. The complete global data set consists of 8741 points, and in view of the structure in the observables that are fit, the number of parameters is not excessive.

Although recoil effects are presumably small for heavy targets this may not be the case for lighter targets. In analyses using the Schrödinger equation the potentials are multiplied by the reduced mass. In the relativistic case there is no unambiguous procedure. As in Ref. [3], we employ the recoil correction given by Cooper and Jennings [5]. This amounts to introducing Cooper-Jennings recoil factors in both scalar and vector potentials. The two factors R_s and R_v multiply the Lorentz scalar and vector optical potentials, respectively. For the scalar potential the Cooper-Jennings factor is

$$R_s = (\text{target mass})/\sqrt{s} , \tag{9}$$

where $\sqrt{s}$ is the total c.m. energy of p-A system. The corresponding Cooper-Jennings factor for the vector potential is

$$R_v = (\text{total c.m. energy of target})/\sqrt{s} . \tag{10}$$

These factors multiply the scalar U_s and vector U_0+V_c, potentials in the Dirac equation,

$$\{\boldsymbol{\alpha}\cdot\mathbf{p}+\beta[m+U_s(r)]+[U_0(r)+V_c(r)]\}\Psi(\mathbf{r})=E\Psi(\mathbf{r}) . \tag{11}$$

The Coulomb potentials V_c is determined from the empirical charge distribution.

For heavy targets these factors are close to unity but for light targets they could have an effect. For example R_v is 0.87 for 800 MeV $p+{}^{12}$C scattering. However, we have found that the global potentials obtained without the Cooper-Jennings recoil factors are quite similar to those obtained when the factors are used. This is understandable since they constitute an additional E and A dependence in the potential strengths which is subsumed in the search. If we turn the recoil factors off and minimize again we find little difference in the resulting χ^2 per degree of freedom. For the individual potential strengths the maximum difference at any energy is at most 10% and less than 1% change in the geometry parameters.

III. DATA ANALYSIS

The references for the data used in this analysis are given in Table I. As in Ref. [3], we restrict the data sets to observables at angles less than 90° in the c.m. or angles corresponding to momentum transfer less than 3 fm^{-1},

TABLE I. Listed are the experimental data sets used in the global searches. In addition the predicted reaction cross sections for each of the fits are also given.

		σ_R(mb)				
			EDAD-fit			
Target	T_p (MeV)	EDAI-fit	fit 1	fit 2	fit 3	Reference
^{12}C	29.00	420.2	435.5	433.1	422.7	[6]
	30.30	415.9	429.0	425.6	414.2	[7]
	49.00	358.8	363.0	348.4	327.7	[6]
	49.48	357.4	361.8	347.0	326.1	[8]
	61.40	323.3	335.6	317.0	294.8	[9]
	65.00	313.5	329.0	309.7	287.4	[10]
	122.00	202.2	269.0	254.4	230.5	[11]
	160.00	177.8	252.3	246.4	215.2	[11]
	200.00	177.6	243.0	243.9	205.0	[11–13]
	300.00	201.1	233.0	235.4	194.9	[14]
	398.00	215.8	227.4	218.6	199.1	[15]
	494.00	227.2	223.7	203.0	211.6	[16]
	797.50	238.4	235.3	209.9	250.0	[17,18]
	1040.00	198.6	259.4	243.8	232.2	[19,20]
^{16}O	23.40	600.1	538.9	549.0	591.9	[21]
	24.20	592.9	533.0	542.4	582.7	[22,23]
	24.50	590.2	530.8	540.0	579.4	[21]
	27.30	566.8	512.7	519.6	550.6	[21]
	27.60	564.4	510.9	517.6	547.8	[22,23]
	30.10	545.5	497.0	501.8	525.4	[21]
	30.40	543.3	495.4	500.0	522.9	[22,23]
	34.10	517.6	477.0	479.1	494.1	[21]
	34.20	517.0	476.6	478.6	493.4	[22,23]
	36.80	500.1	465.0	465.4	475.6	[21]
	37.10	498.2	463.7	464.0	473.7	[22,23]
	39.70	482.4	453.1	451.9	457.8	[21]
	40.00	480.6	452.0	450.6	456.0	[22,23]
	43.10	462.9	440.5	437.5	439.2	[21]
	46.10	446.9	430.5	426.0	424.8	[21]
	65.00	367.1	383.0	372.3	364.3	[10,24]
	100.60	288.3	333.7	321.5	320.5	[25]
	135.00	260.8	309.9	301.9	305.3	[26]
	179.90	252.8	295.1	292.6	293.6	[27]
	317.50	260.4	283.3	275.3	268.0	[28]
	498.00	277.4	282.0	250.0	269.1	[29,30]
	650.00	296.1	294.2	257.8	296.9	[29,30]
	800.00	304.7	316.3	289.6	323.0	[31,32]
	1040.00	284.2	351.9	339.1	323.6	[33]
^{24}Mg	65.00	· · ·	498.5	489.8	489.8	[24]
^{28}Si	65.00	· · ·	550.1	538.8	543.3	[24]
^{40}Ca	21.00	894.0	891.4	883.4	893.5	[34,35]
	23.50	883.7	885.4	878.2	882.7	[36]
	25.00	875.9	878.7	871.7	874.3	[36]
	26.30	868.0	871.5	864.4	866.0	[36,37]
	27.50	860.4	864.0	857.0	857.7	[36]
	30.00	844.0	848.1	840.8	840.1	[36,37]
	35.00	814.0	818.3	810.9	807.8	[36,38]
	40.00	788.2	791.1	783.5	780.0	[36,39]
	45.00	766.1	766.2	758.6	756.1	[36,38]

TABLE I. (*Continued*).

		σ_R(mb)				
			EDAD-fit			
Target	T_p (MeV)	EDAI-fit	fit 1	fit 2	fit 3	Reference
	48.00	754.4	752.5	745.0	743.4	[36,40]
	65.00	705.3	690.3	685.3	690.9	[41]
	80.00	676.4	652.0	651.2	661.9	[42,43]
	100.00	647.0	616.9	622.8	636.0	[25]
	135.00	607.0	581.5	598.7	606.5	[43]
	160.00	584.6	567.6	590.8	591.7	[42,43]
	181.30	569.2	560.0	586.4	581.9	[43]
	200.00	558.5	555.2	583.3	575.1	[13]
	318.00	531.5	539.4	461.3	559.4	[44]
	362.00	531.6	536.0	552.0	561.4	[45]
	400.00	534.3	534.3	545.1	565.0	[46]
	497.50	550.4	538.4	537.9	580.0	[47–49]
	613.00	580.4	560.0	555.3	603.4	[33]
	650.00	590.4	570.0	565.9	611.2	[29]
	797.50	622.1	613.9	615.3	636.5	[50–52]
	1044.00	639.6	662.0	647.3	634.5	[20,53]
^{48}Ca	65.00	· · ·	788.2	791.4	793.4	[41]
	497.50	· · ·	607.2	602.3	646.1	[47]
	797.50	· · ·	686.9	681.6	708.3	[50]
	1044.00	· · ·	736.0	707.9	715.5	[53]
^{56}Fe	65.00	· · ·	868.1	877.9	878.0	[24]
^{60}Ni	65.00	· · ·	909.3	921.1	921.1	[24]
^{90}Zr	22.50	1348.9	1285.9	1300.4	1309.3	[54]
	40.00	1348.5	1315.2	1334.5	1336.1	[36,39]
	61.40	1230.6	1223.6	1233.5	1244.7	[9]
	65.00	1212.4	1208.8	1216.9	1229.3	[41]
	80.00	1147.5	1154.8	1156.5	1171.4	[42,43]
	135.00	1017.2	1043.0	1042.0	1031.7	[43]
	160.00	985.5	1019.0	1021.1	993.2	[42,43]
	182.00	963.9	1004.5	1009.2	967.9	[43]
	500.00	943.0	930.0	923.4	955.2	[47]
	800.00	1022.4	1033.4	1039.2	1067.7	[55]
^{208}Pb	21.00	1474.6	1451.0	1478.3	1521.6	[56]
	24.10	1645.1	1623.9	1647.8	1687.0	[56]
	26.30	1737.8	1718.7	1738.1	1774.3	[56]
	30.50	1869.7	1855.7	1866.6	1899.9	[56]
	35.00	1962.3	1950.1	1956.7	1985.5	[56]
	40.00	2031.3	2020.3	2022.1	2046.6	[56]
	65.00	2077.2	2079.6	2063.0	2084.1	[41]
	80.00	2022.6	2039.7	2009.5	2034.2	[42,43]
	121.20	1866.6	1924.8	1873.5	1895.4	[43]
	160.00	1782.4	1859.8	1087.2	1809.0	[42,43]
	182.40	1755.4	1837.0	1786.5	1775.8	[42,43]
	200.00	1740.5	1822.6	1774.0	1754.8	[46]
	400.00	1682.1	1719.1	1684.8	1694.5	[46]
	497.50	1703.2	1711.3	1685.9	1703.2	[47–49]
	797.50	1805.0	1872.6	1897.0	1803.4	[51,52,57]
	1040.00	1909.8	1918.9	1958.1	2169.4	[19,20]

whichever is smaller. This is done because nonlocalities in the optical model potential are presumably important at large angles. Systematic errors are approximated by adding 3% of the cross section in quadrature to the quoted experimental error. For the spin observables A_y and Q, 0.02 is added in quadrature to the quoted errors. In order to give each data set roughly equal standing in the fitting procedure we divided the χ^2 for each observable in a data set by the number of data points in that data set. The function minimized is given by

$$\chi^2=\sum_{j=1}^{N_s}[\chi^2_\sigma(j)+\chi^2_{A_y}(j)+\chi^2_Q(j)]\ , \tag{12}$$

where N_s is the total number of data sets in the search. The individual χ^2's for each data set are given by

$$\chi^2_\sigma=\frac{1}{N_\sigma}\sum_{i=1}^{N_\sigma}\left[\frac{F_N\sigma_{\text{expt}}(i)-\sigma_{\text{calc}}(i)}{\Delta\sigma(i)}\right]^2\ , \tag{13a}$$

$$\chi^2_{A_y}=\frac{1}{N_{A_y}}\sum_{i=1}^{N_{A_y}}\left[\frac{A_{y_{\text{expt}}}(i)-A_{y_{\text{calc}}}(i)}{\Delta A_y(i)}\right]^2\ , \tag{13b}$$

and

$$\chi^2_Q=\frac{1}{N_Q}\sum_{i=1}^{N_Q}\left[\frac{Q_{\text{expt}}(i)-Q_{\text{calc}}(i)}{\Delta Q(i)}\right]^2\ . \tag{13c}$$

Here N_σ is the number of cross section points in data set j, similarly for N_{A_y} and N_Q. The normalization of the cross section data F_N is searched on. The expression for F_N is

$$F_N=\frac{\sum_{i=1}^{N_\sigma}\{\sigma_{\text{calc}}(i)\sigma_{\text{expt}}(i)/[\Delta\sigma(i)]^2\}}{\sum_{i=1}^{N_\sigma}\{[\sigma_{\text{expt}}(i)]^2/[\Delta\sigma(i)]^2\}}\ . \tag{14}$$

IV. RESULTS OF THE ANALYSES

The goal of the A-independent analysis was to provide high-quality energy-dependent optical potentials for each of the following targets: ^{12}C, ^{16}O, ^{40}Ca, ^{90}Zr, and ^{208}Pb. These fits are called the E-dependent–A-independent (EDAI) fits. From the general form of the model given in Eq. (1) one has a total of eight potentials which are functions only of energy and radius in this case. No cross terms are included; in addition no surface peaked terms are included in the real potentials and the shape parameters R and a are taken to be the same in the surface peaked imaginary potentials as in the volume imaginary potentials. Thus, the total number of parameters varied in each fit is 70. The number of data points for every target is well over 1000.

The EDAI fits obtained are of high quality over the range of data included in the fit. The agreement with experiment for heavy targets is comparable to or better than those shown in Ref. [3]. A comparison of the global results with single energy fits using the standard 12 parameter SV model of Dirac phenomenology [58–63], shows that the calculated observables are in very good agreement over the q^2 range covered in the global work. The results for the global fits for each target are even more impressive when one notes that the total χ^2 per degree of freedom given by

$$\chi^2_{\text{pdf}}=\frac{1}{N-N_p}\sum_{j=1}^{N_s}[N_\sigma(j)\chi^2_\sigma(j)+N_{A_y}(j)\chi^2_{A_y}(j)+N_Q(j)\chi^2_q(j)]\ , \tag{15}$$

is less than 3.9, a value for χ^2/N which would indicate that an acceptable fit had been achieved in an analysis of data at only a single energy. In Eq. (15), N is the total number of data points in the search and N_p is the number of searched parameters.

The expansion coefficients, v_n, r_n, and a_n, determined from the fits for each target are tabulated in Ref. [64]. The EDAI potentials are included in the computer program GLOBAL [65] which produces the scalar and vector potentials, as well as the Schrödinger equivalent (SE) potentials obtained from them [58–61]. The EDAI potentials interpolate well in energy, and if the results are needed for a nearby target, i.e., ^{13}C or ^{42}Ca, an $A^{1/3}$ scaling of the geometry parameters gives reasonable results. However, as with all global potentials, extrapolation in energy should be avoided.

The full E- and A-dependent analysis presented a considerable challenge because of the inclusion of light target data as well as the extension to low energies. Almost all global treatments, regardless of energy range, are restricted to heavy targets. No previous global optical potential covers such a large energy and target mass range. In spite of the good fits obtained in this work we continue to search for better parametrization and improved fitting procedures.

In this work we present three different E- and A-dependent global potentials, termed EDAD fits 1, 2, and 3. This allows the user to test the sensitivity of the computation to the input optical model potentials. All three give high-quality agreement with the available data. The number of parameters and the form of the potential changes from fit to fit. In the first, EDAD fit 1, the cross terms in Eqs. (6)–(8) are absent; there is no surface peaked term in the real potentials and no A dependence in the imaginary surface peaked terms. In this case 106 parameters are varied and the resulting χ^2 divided by the number of degrees of freedom is 6.0. As was the case for the first fit, the next two fits start from random parameters. The inclusion of the cross terms and A dependence in the imaginary surface peaked terms increases the number of parameters to 154 and the resulting χ^2 per degree of freedom is 5.1. The final fit presented here, EDAD fit 3, contained 176 parameters and achieved a χ^2 per degree of freedom of 4.6. The EDAD fit 3 exhibits some lack of systematics for the imaginary scalar and vector potentials due to the presence of the surface peaking in the real potentials. These defects, which are only apparent for ^{208}Pb at energies above 500 MeV, lead us to suggest that this fit only be used for testing sensitivity to the optical model. In fact, as the EDAI fits produce, not unexpectedly, slightly better quality fits to experiment we suggest that

these fits be used when comparing with microscopic models. The expansion coefficients for all of the EDAD fits are given in Ref. [64].

The interpolation in properties of the EDAD fits are reasonable; predicted observables for the heavy targets are of the same quality as those given in Ref. [3] and are generally almost as good as the results obtained from the EDAI fits for the five spin-zero targets included in the EDAI investigation. As our previous global potentials did not include light targets, we show in Figs. 1 and 2 typical examples of the quality of the predictions when E- and A-interpolation is required. If the optical potential needed corresponds to one of the targets used in the A-independent fits then our recommendation is to use the EDAI potentials as the fits are somewhat better and then use the EDAD fits to check for optical model sensitivity. In the event that a substantial interpolation in A is required we urge caution. It is always prudent to try to check with existing data if at all possible. In addition, as discussed in Ref. [3], the model is not suitable for strong-

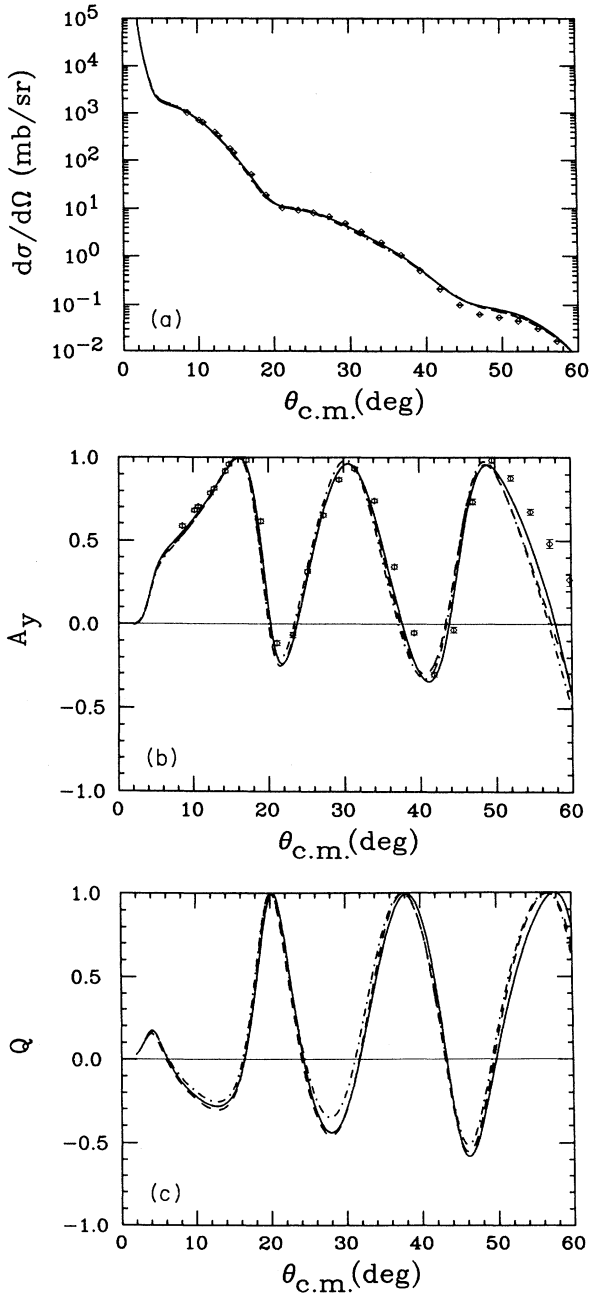

FIG. 1. The observables predicted for 179 MeV protons elastically scattered from ^{28}Si using EDAD fit 1 (solid line), EDAD fit 2 (dashed line) and EDAD fit 3 (dash-dot line) potentials. The data are from Ref. [66].

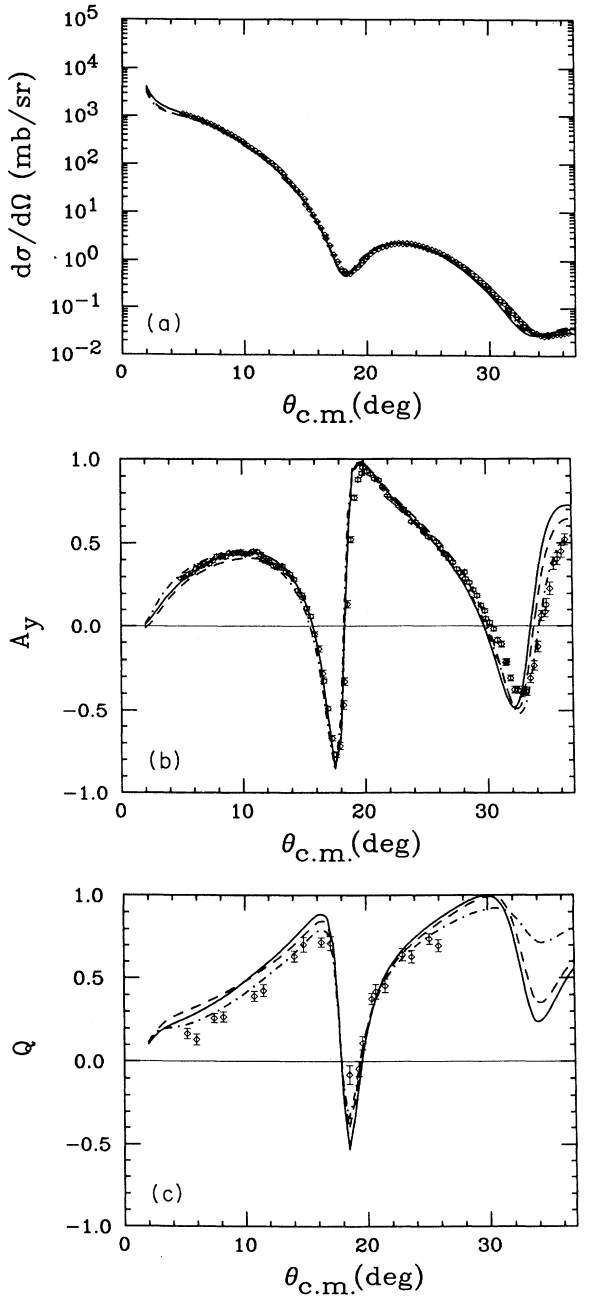

FIG. 2. The observables predicted for 494 MeV protons elastically scattered from ^{13}C using EDAD fit 1 (solid line), EDAD fit 2 (dashed line) and EDAD fit 3 (dash-dot line) potentials. The data are from Ref. [16].

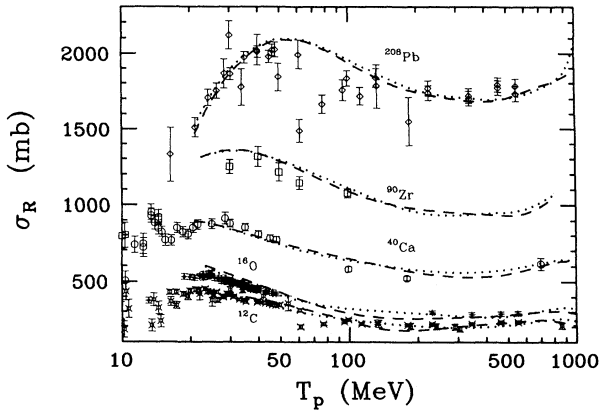

FIG. 3. The calculated reaction cross sections predicted by the EDAI global potentials (dashed line) and the EDAD fit 3 (dotted line). T_p is the proton kinetic energy. The data are from Ref. [67].

ly deformed targets. The program GLOBAL [65] generates the scalar and vector Dirac potentials as well as the Schrödinger equivalent (SE) potentials obtained from them for any of the fits discussed in Ref. [3] and in this paper.

Table I gives the predicted reaction cross sections for the EDAI and EDAD optical models. The agreement is generally within the experimental error where measured reaction cross sections exist. We show the predicted reaction cross sections along with the experimental data in Fig. 3. It is obvious that there is a great need for improved measurements of the reaction cross sections for a wide range of targets and energies. The total neutron cross section are predicted from the EDAI and EDAD potentials with the Coulomb potential set to zero. No Coulomb energy shift is made. The results are shown in Fig. 4, and as would be expected, the agreement with the empirical values worsens as the neutron excess increases. Encouraged by these results and by the recent work of Kozack and Madland [71,72] and Varner *et al.* [73] we

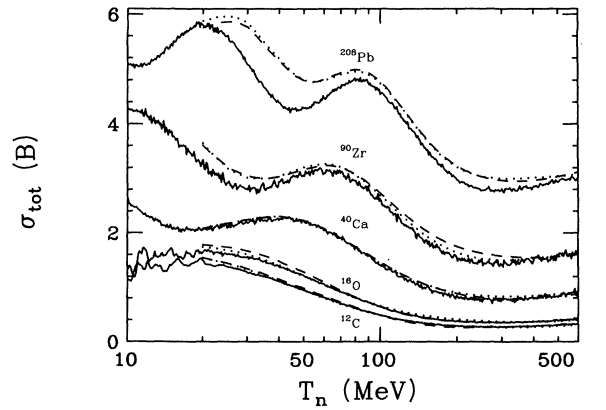

FIG. 4. The calculated total neutron cross sections predicted from the EDAI global potentials (dashed line) and the EDAD fit 3 (dotted line). T_n is the neutron kinetic energy. The data are from Refs. [68–70].

have started a program to determine the global Dirac optical model isovector and isoscalar potentials for heavy targets.

The real parts of the EDAI and EDAD scalar and vector optical potentials exhibit very systematic behavior with energy for all targets. As expected, the imaginary parts of the scalar and vector potentials are somewhat less systematic due to the presence of the surface peaking term. Comparison of the potentials for the light targets, ^{12}C and ^{16}O, with those for the heavier targets shows the increased importance of the surface terms for the former. For example, except for the case of ^{208}Pb, the imaginary scalar and vector potentials exhibit considerable surface peaking at low energies which persists up to 100 MeV. At energies below 60 MeV the interior of the imaginary potentials is not well determined due to the competition between surface and volume terms. Figure 5 shows the potentials for ^{208}Pb obtained from the EDAI fit, similar behavior is obtained for the A-dependent global fits. Figures showing the EDAI potentials as well as examples of the EDAD fit 3 potentials are given in Ref. [64]. It is apparent from Fig. 5 that the potential shapes are characterized by a volume form and that the effect of surface peaking is small although still present at the lowest ener-

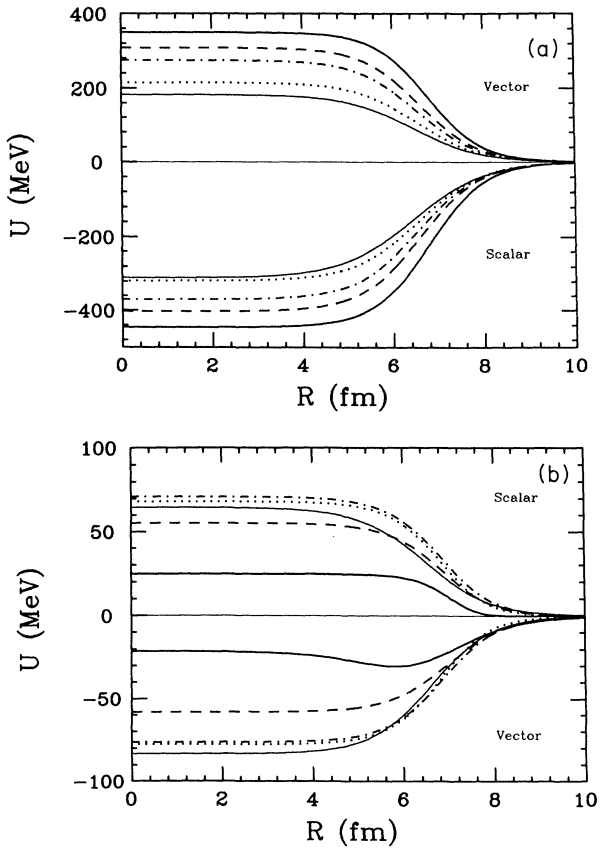

FIG. 5. The real scalar and vector optical potentials calculated for ^{208}Pb using the EDAI global potentials evaluated at T_p equal 20 MeV (thick solid line), 100 MeV (dashed line), 200 MeV (dot-dashed line), 500 MeV (dotted line), and 800 MeV (thin solid line) are shown in (a), the corresponding imaginary parts are shown in (b).

gies. This is in agreement with the E- and A-dependent analysis given in Ref. [3]. The corresponding SE potentials are shown in Fig. 6. One feature of the SE spin-orbit potential is noteworthy; we find that the magnitude of the maximum value of these potentials to exhibit considerable A dependence. For example, the values for ^{12}C are roughly a factor of 3 larger then those for ^{208}Pb. We also note that the imaginary part of the spin-orbit potential is not well determined in the interior at energies below 60 MeV. The central SE potential exhibits many of the characteristics of microscopic nonrelativistic or relativistic potentials, such as the "wine-bottle" shape of the real central SE potential, its change from an attractive potential to a repulsive one in the transition energy region around 300 MeV, and the surface peaking of the imaginary potentials at low energies [74–77]. For example, the relativistic Dirac-Bruekner calculations of ter Haar and Malfliet [77] produce a real central SE potential for normal nuclear matter density which passes through zero around 300 MeV. The volume integral of the real central SE potential for ^{208}Pb is zero at 315 MeV, in remarkable agreement with their results. In addition, the values of the SE central real and imaginary potentials at the origin agree quite well with the Dirac-Brueckner calculations. Figures of the SE potentials for all of the EDAI fits as well as examples of the EDAD fit 3 potentials are given in Ref. [64].

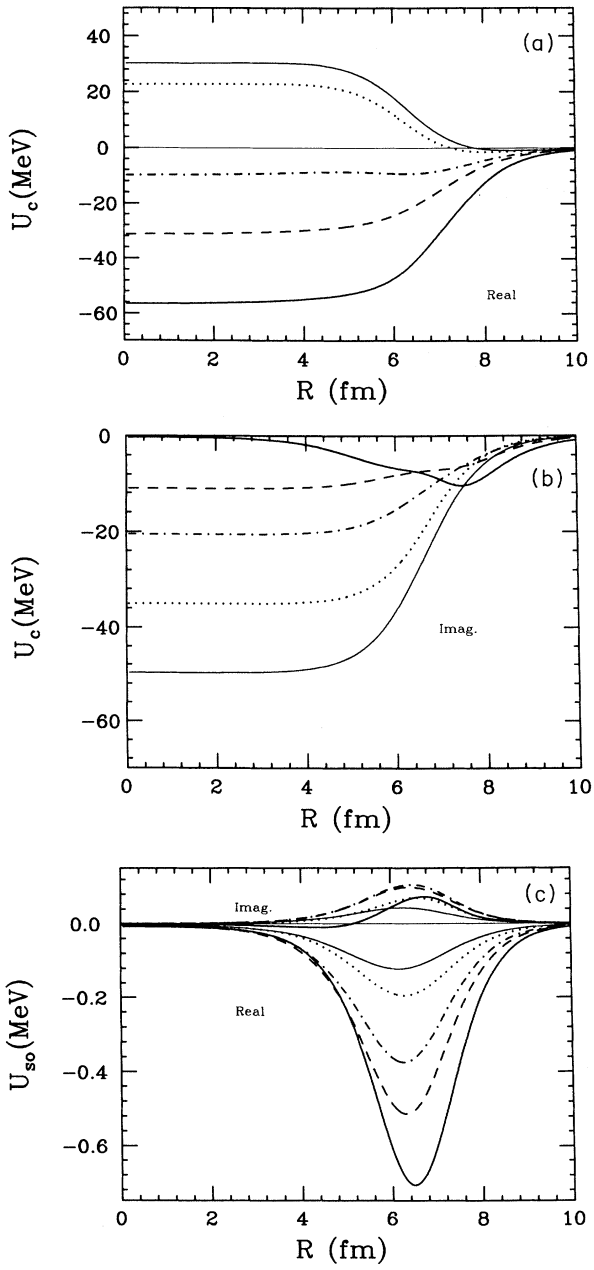

FIG. 6. The SE real central potential calculated from potentials in Fig. 5 are shown in (a). The SE imaginary potentials calculated from the potentials in Fig. 5 are shown in (b). The real and imaginary SE spin-orbit potentials calculated from the potentials in Fig. 5 are shown in (c).

As discussed in Ref. [3] the global optical potentials obtained in that work were in reasonable agreement with the relativistic impulse approximation (RIA) calculations of Refs. [78] and [79] at energies above 300 MeV, see Figs. 9 and 10 of Ref. [3]. Here we also compare our results with the case 2 relativistic impulse approximation (IA2) potentials of Ottenstein, Wallace, and Tjon [80]. The classic example is ^{40}Ca at 500 MeV and in Fig. 7 we show the scalar and vector potentials and the SE central and spin-orbit potentials obtained from them for the RIA [78], the IA2 [80] and the EDAI global fit for ^{40}Ca at 500 MeV. The IA2 scalar and vector potentials are smaller than either the RIA and EDAI global potentials, which agree quite well with each other. This may not be surprising as the IA2 potential contains an explicit $\sigma \cdot L$ term absent from the RIA and the phenomenological potentials. The RIA and IA2 potentials both contain tensor terms which arise from the strong and electromagnetic interactions, while the phenomenology contains only scalar and vector potentials; we find that the inclusion of the tensor anomalous moment term does not significantly alter the parameters. We do not attribute the difference between the scalar and vector IA2 and EDAI global potentials to the analytic form of the global potentials which exhibit little structure in the nuclear interior. We observe a similar discrepancy with the IA2 results when the global optical model is constrained by relativistic Hartree potentials as was done in Ref. [81]. In these fits the geometry of the real optical potentials is held fixed throughout the search. As described in Ref. [81], the real optical potentials are calculated using relativistic Hartree mean-field densities equal to those used in the IA2 optical model calculations of Ref. [80]; and the imaginary scalar and vector potentials had SWS form factors. Rather, we feel that the differences may be due to the additional terms in the IA2 potential. That this is plausible may be seen from a comparison of the SE IA2 potentials, which contain all of the terms [80], with the RIA and global potentials. Figures 7(b) and 7(c) show that the SE potentials are similar except for the behavior of the spin-orbit potentials inside 2 fm. One cause of this difference is that the global potentials have zero derivatives at the origin while the IA2 and RIA do not. The more important

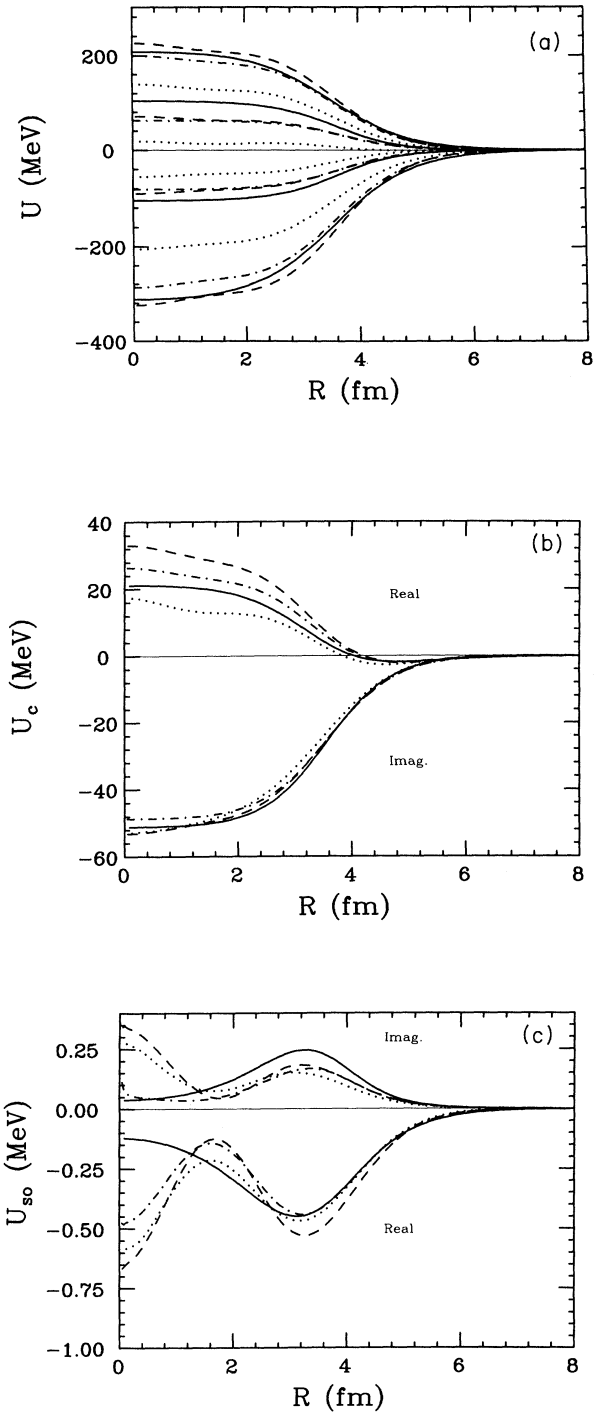

FIG. 7. (a) shows the scalar and vector optical model potentials for 500 MeV protons scattered elastically from ^{40}Ca calculated using the EDAI global fit (solid line), the RIA [78] (dashed line), the IA2 [80] (dotted line), and the potentials of Ref. [81] (dot-dashed line). In order of decreasing values of the potential strengths at the origin, the first four curves show the real vector potentials, the next four the imaginary scalar potentials, the next four the imaginary vector potentials and the final four the real scalar potentials. (b) and (c) show the corresponding SE potentials calculated from the scalar and vector potentials shown in (a).

cause is the structure in the scalar and vector potentials produced by the relativistic mean-field densities. The real spin-orbit SE potential obtained using the constrained potentials of Ref. [80] shows similar behavior to real spin-orbit IA2 and RIA potentials inside 2 fm, while the imaginary spin-orbit potential resembles the global potential. Because the IA2 potentials are the most complete microscopic relativistic optical potentials available we plan to construct a global potential based on them. We will then be able to investigate the optical potentials determined from using the IA2 potentials as a constraint in a similar manner to that done in Ref. [81].

It has been observed that the moments of the optical potential are generally well determined [3]. In Ref. [3] we showed a number of the moments of the scalar and vector potentials as well as the SE potentials obtained from them. The global fits presented here exhibit essentially the same dependence so we do not show them again. We do note the following features of the real scalar and vector potentials. The volume integrals of the real scalar and vector potentials divided by the target mass number, J_v/A and J_s/A, show little A dependence. The energy dependence of J_v/A and J_s/A is similar for all targets, the decrease in the volume integrals with increasing energy is essentially as shown in Fig. 29 of Ref. [3]. The corresponding rms radii divided by $A^{1/3}$ have little energy dependence, especially for the heavy targets as is shown in Figs. 8 and 9. Above 200 MeV the values are essentially constant. The EDAD fits show even smaller energy dependence than the EDAI fits due to the additional constraint of the A dependence. Table II gives the average values for the rms radii from the EDAI fits for each of the targets along with the standard deviation. As we found in the early work using Dirac phenomenology, we find that the ratio J_v/J_s has a simple linear energy dependence, and at low energy approaches the value 0.8, expected from the Walecka model [58,82]. Turning to the imaginary scalar and vector potentials we find, as expected, that the moments of the imaginary scalar and vector potentials exhibit more dependence on target mass

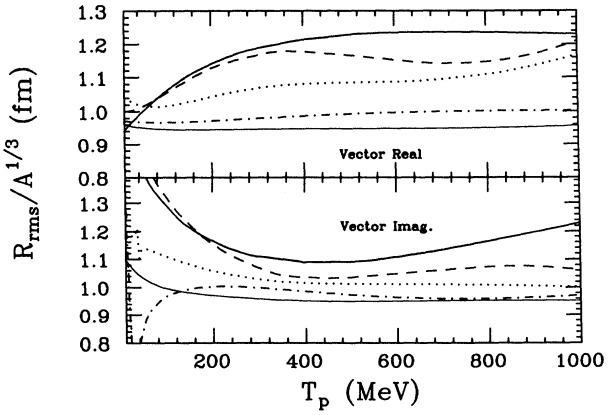

FIG. 8. The real and imaginary rms radii divided by $A^{1/3}$ of the vector EDAI global potentials. T_p is the proton kinetic energy. The targets are ^{12}C (thick solid line, the top line), ^{16}O (dashed line), ^{40}Ca (dotted line), ^{90}Zr (dot-dashed line), and ^{208}Pb (thin solid line, the bottom line).

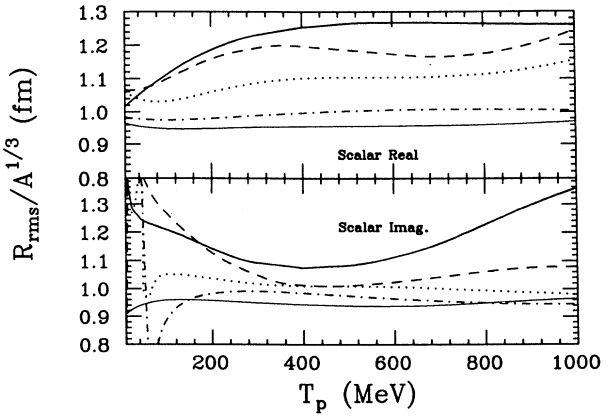

FIG. 9. The real and imaginary rms radii divided by $A^{1/3}$ of the scalar EDAI global potentials. T_p is the proton kinetic energy. The targets are ^{12}C (thick solid line, the top line), ^{16}O (dashed line), ^{40}Ca (dotted line), ^{90}Zr (dot-dashed line), and ^{208}Pb (thin solid line, the bottom line).

and energy, but are generally systematic. For example, as shown in Figs. 8 and 9, the rms radii divided by $A^{1/3}$ exhibit considerable energy dependence below 80 MeV due to the competition between surface and volume absorption, but are relatively energy independent at higher energies. It is well known that the real potentials are better determined than the imaginary potentials, especially at low energies.

Next we discuss moments of the real and imaginary SE central and spin-orbit potentials. As discussed above, the energy at which the real SE J/A for ^{208}Pb passes through zero is in remarkable agreement with the relativistic Dirac-Brueckner calculations of Ref. [77]. We find that the energy at which the real SE J/A is zero is A dependent, for example it is zero at 315 MeV for ^{208}Pb and at 650 MeV for ^{12}C. The value of the energy at which the real part of J/A is zero exhibits saturation with increasing A, so that the energy at which J/A is zero for ^{208}Pb is a reasonable approximation to the corresponding value

TABLE II. The average values of the rms radii of scalar and vector optical potentials divided by $A^{1/3}$ from the EDAI global fit. The imaginary values are calculated from the results above 100 MeV.

Target		real (fm)	imag. (fm)
^{12}C	scalar	1.2276±0.0629	1.1660±0.0851
	vector	1.1893±0.0723	1.1467±0.0515
^{16}O	scalar	1.1711±0.0391	1.0651±0.0584
	vector	1.1424±0.0471	1.0832±0.0631
^{40}Ca	scalar	1.0950±0.0313	1.0094±0.0184
	vector	1.0826±0.0383	1.0236±0.0256
^{90}Zr	scalar	0.9966±0.0118	0.9637±0.0205
	vector	0.9886±0.0129	0.9759±0.0154
^{208}Pb	scalar	0.9569±0.0057	0.9485±0.0085
	vector	0.9485±0.0031	0.9570±0.0108

in nuclear matter. The volume integrals of the SE spin-orbit potentials, $K/A^{1/3}$, indicate that the real part dominates the imaginary spin orbit. The imaginary spin-orbit volume integral is small at low energies and takes on its maximum value around 200 MeV for all targets. However, the imaginary part, which cannot be eliminated in a relativistic model, is critical to the fit, even at low energies. The real SE spin-orbit rms radii divided by $A^{1/3}$ are remarkably independent of energy and A from 20 to 1000 MeV. The same is true of the real central rms radii divided by $A^{1/3}$ up to the transition energy; beyond that it exhibits large energy dependence as J/A changes sign. The imaginary SE spin-orbit rms radius divided by $A^{1/3}$ has very little dependence on the energy and A beyond 80 MeV. The values at lower energies reflect the underlying competition between surface and volume absorption in the scalar and vector imaginary potentials and thus exhibit considerable energy dependence. The behavior of the various moments of the scalar and vector potentials, and the SE potentials obtained from them, is given in Ref. [64].

In addition to the moments of the global potentials discussed above, it is possible to extract other quantities which provide a useful source of comparison with relativistic and nonrelativistic treatments of the nuclear optical potential. Some of these will be the subject of a separate paper. Here we discuss the mean free path λ, the usual nonrelativistic effective mass m_e^*, the Dirac mass $M^*=m+S(r,E,A)$, where m is the nucleon mass, and the effective energy shift, $E^*=E-V(r,E,A)$, where E is the projectile energy.

Starting with the work of Bethe [83] in 1940 there has been considerable interest in the determination of the mean free path of a proton or neutron in the nuclear medium. This quantity is also of interest in both relativistic and nonrelativistic nuclear many-body theory. Recent work in the area of nuclear transparency has increased the need for a reliable empirical determination of the mean free path [84]. As discussed by Negele and Yazaki [85] the appropriate nonrelativistic expression for the energy dispersion for finite nuclei described by a local energy-dependent optical model potential is

$$T_p=\frac{k^2}{2m}+U_{\rm opt}(r,E)\ , \tag{16}$$

where k is complex. The mean free path is defined as

$$\lambda=\frac{1}{2\,{\rm Im}k}\ . \tag{17}$$

In this case the real and imaginary SE potentials determined from the global fits can be used in Eq. (16). Note that the mean free path is a function of both energy and the radius, and that the value of λ is quite sensitive to the choice of the radius.

Alternatively, we can use the relativistic expression given by Cheon [86], where the global scalar and vector potentials are used in the dispersion relations given by

$$E=\{[m+S(r,E)]^2+k^2\}^{1/2}+V(r,E)\ . \tag{18}$$

Again, the mean free path is given by Eq. (17). In calculating the mean free path we use the EDAI optical potentials for ^{208}Pb with the radius taken to be 0, 5, and 6 fm.

We calculate k using either Eq. (16) or (18), and the values for λ for both cases are shown in Fig. 10. There is little difference between the results obtained for $r=0$ and 5 fm as the potentials for ^{208}Pb are quite flat in this region. The matter density at 5 fm, calculated from the electron scattering charge distribution, is 0.16 fm^{-3} corresponding to that of normal nuclear matter, while that at 6 fm is more characteristic of the nuclear surface. It is clear that there is considerable difference between the calculations with $r=5$ and 6 fm. While proton elastic scattering data does not determine the interior of the optical potential, the wine-bottle shape of the real SE potential, required by the data, indicates that they are reliable outside $r \geq 4$ fm. Thus, we feel justified in using our results to give a measure of the empirical mean free path in the nuclear medium and to give good estimates of its value in nuclear matter. If comparison is to be made between optical model results and other types of determinations of the mean free path, especially those for nuclear matter, the radius should be chosen to correspond to nuclear matter density.

The standard approach for determining an empirical mean path has been to use measured reaction cross sections for many targets at a spread of energies. Using a simple model first introduced in 1940 by Bethe [83] an approximation to the mean free path is found, see Renberg *et al.* [87]. In the work of Nadasen *et al.* [43] the reaction cross section was calculated from an optical model analysis of proton elastic scattering data in the range 80–180 MeV. However, the calculation for the mean free path was subject to uncertainties in the optical model potentials. We agree with the observation of Meyer and Schwandt [88] that the empirical mean free path can only be determined from optical model potentials that are well determined. Our results differ from those of Nadasen *et al.* particularly with respect to the energy dependence of the mean free path. It is our contention that reliable empirical values of the mean free path may be obtained from the global optical model potentials described herein. The potentials reported in this work are free from serious ambiguities due to the extensive energy region considered and the large data set included in the fits. There remains, however, the question of the choice of the value of the optical model radius at which λ is evaluated. In a separate paper we discuss this question and compare the mean free path obtained from the global potentials with those obtained from recent measurements of the total neutron-nucleus cross sections [68–70,89].

There are a plethora of effective masses discussed in the literature. The paper by Jaminon and Mahaux has provided a welcome discussion of the various definitions of the quantities in current use [90]. In this paper we consider the two quantities defined above, M^* and E^*, commonly used in relativistic nuclear physics, and the nonrelativistic-type effective mass m_e^* given in Ref. [90],

$$m_e^* = m\left[1-\frac{dV_e(E,r)}{dE}\right] . \tag{19}$$

In Eq. (19), $V_e(E,r)$ is the real part of the SE potential as defined in Ref. [58] which differs slightly from that used by Jaminon and Mahaux. Here we use the full SE potential obtained from the reduction of the Dirac equation to second order form. And, as in the calculation for λ above, we use the EDAI fit for ^{208}Pb calculated at $r=0$, 5, and 6 fm. For comparison with microscopic relativistic nuclear matter calculations, such as those of ter Haar and Malfliet, it is appropriate to evaluate the global potentials at the radius corresponding to nuclear matter density.

In Figs. 11 and 12 we show the energy dependence of M^* and E^* calculated using the EDAI fit for the heaviest target, ^{208}Pb. The energy dependence of both quantities is expected as the scalar and vector potentials both decrease in magnitude with increasing energy. At low energies the value of M^*/m calculated at 5 fm is in good agreement with the calculations of ter Haar and Malfliet [77]. In Fig. 13 the ratio m_e^*/m is given as a function of

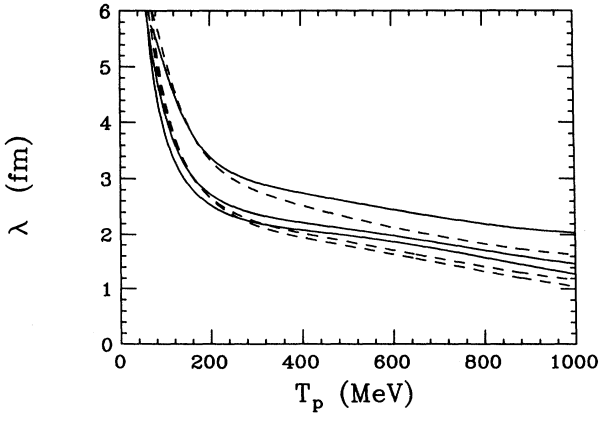

FIG. 10. The mean free path calculated using Eqs. (16) (dashed line) and (18) (solid line) vs the proton kinetic energy. The EDAI optical potentials for ^{208}Pb are evaluated at $r=0$, 5, and 6 fm, the resulting λ values increase as the value of r increases. T_p is the proton kinetic energy.

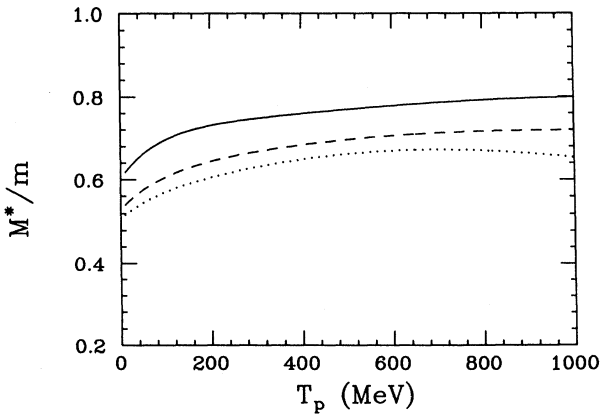

FIG. 11. The ratio of the Dirac mass to the proton mass calculated using the EDAI global scalar potential for ^{208}Pb evaluated at $r=0$ fm (dotted line), $r=5$ fm (dashed line), and $r=6$ fm (solid line). T_p is the proton kinetic energy.

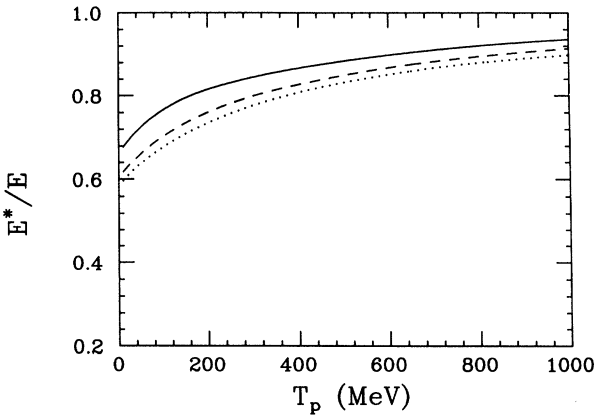

FIG. 12. The ratio of the relativistic energy shift E^* to the total energy of the proton in the center of momentum frame calculated using the EDAI global vector potential for ^{208}Pb evaluated at $r=0$ fm (dotted line), $r=5$ fm (dashed line), and $r=6$ fm (solid line). T_p is the proton kinetic energy.

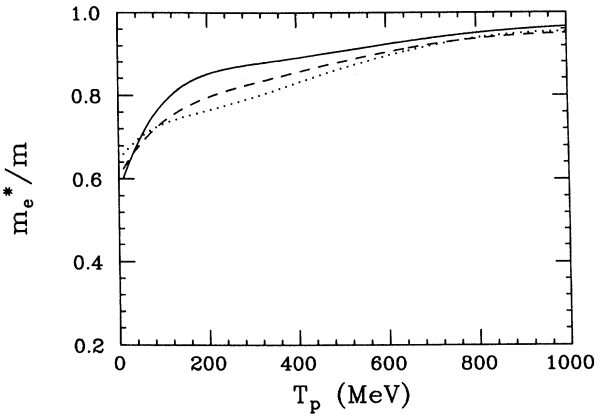

FIG. 13. The ratio of the effective mass defined by Eq. (19) to the proton mass calculated using the EDAI global SE central potential for ^{208}Pb evaluated at $r=0$ fm (dotted line), $r=5$ fm (dashed line), and $r=6$ fm (solid line). T_p is the proton kinetic energy.

energy and the low-energy values for the calculation at 5 fm are in good agreement with the results in Ref. [77]. Additional comparisons of the global potentials and nonrelativistic and relativistic microscopic calculations will be the subject of a subsequent paper. The results to date indicate the value of these global potentials as a testing ground for such calculations.

V. SUMMARY

In summary, we have presented the most recent results of the program to obtain global optical model potentials for a wide range of uses. We find that the potentials are systematic and that the scalar and vector potentials as well as the Schrödinger equivalent potentials obtained from them exhibit many of the characteristics of relativistic and nonrelativistic microscopic optical potentials. The energy and A dependence of the various moments of the scalar and vector potentials as well as the SE potentials are investigated and shown to be remarkably systematic. This fact confirms their suitability as the empirical optical potentials for use in checking microscopic calculations.

We further suggest that these global potentials, when used in the energy momentum dispersion relation, provide reliable empirical values for the mean free path of a nucleon in the nuclear medium. In addition, they provide reliable empirical values for quantities of interest in nuclear many-body physics, such as the relativistic effective mass M^* and the corresponding effective energy shift E^* as well as the usual effective mass m_e^*.

We continue to improve both the data base and the optical model and as the improved results become available they will be provided to the nuclear community. The Addendum to this paper [64] provides tables of the optical model expansion coefficients, figures showing the global optical model potentials at a number of energies, figures of some of the characteristic features of these potentials, and examples of the quality of the predictions of elastic proton scattering observables obtained from them. The current potentials are available from the authors in convenient form from the program GLOBAL [65].

ACKNOWLEDGMENTS

We thank R. Finlay, R. Furnstahl, C. Mahaux, and D. Wasson for useful discussions. We also thank R. Finlay for providing the neutron total cross section data prior to publication. This work was supported in part by National Science Foundation Grants Nos. Phys-8822550, Phy-9207889, and Phy-9202836, The Ohio Supercomputer Center, and a Seed Grant from The Ohio State University.

[1] E. D. Cooper, B. C. Clark, R. Kozack, S. Shim, S. Hama, J. I. Johansson, H. S. Sherif, R. L. Mercer, and B. D. Serot, Phys. Rev. C **36**, 2170 (1987).
[2] E. D. Cooper, B. C. Clark, S. Hama, and R. L. Mercer, Phys. Lett. B **206**, 588 (1988); **220**, 658(E) (1989).
[3] S. Hama, B. C. Clark, E. D. Cooper, H. S. Sherif, and R. L. Mercer, Phys. Rev. C **41**, 2737 (1990).
[4] T. D. Cohen, R. J. Furnstahl, and D. K. Griegel, Phys. Rev. Lett. **67**, 961 (1991).
[5] E. D. Cooper and B. K. Jennings, Nucl. Phys. **A483**, 601 (1988).
[6] R. M. Craig, J. C. Dore, G. W. Greenlees, J. Lowe, and D. L. Watson, Nucl. Phys. **83**, 493 (1966).
[7] B. W. Ridley and J. F. Turner, Nucl. Phys. **58**, 497 (1964).
[8] J. A. Fannon, E. J. Burge, D. A. Smith, and K. N. Ganguly, Nucl. Phys. **A97**, 263 (1967).

[9] C. B. Fulmer, J. B. Ball, A. Scott, and M. L. Whiten, Phys. Rev. **181**, 1565 (1969).

[10] H. Sakaguchi, M. Yosoi, M. Nakamura, T. Noro, H. Sakamoto, T. Ichihara, M. Ieiri, Y. Takeuchi, H. Togawa, T. Tsutsumi, H. Ikegami, and S. Kobayashi, in *Proceedings of the Sixth International Symposium on Polarization Phenomena in Nuclear Physics, Osaka, 1985,* edited by M. Kondo, S. Kobayashi, M. Tanifuji, T. Yamazaki, K.-I. Kubo, and N. Onishi [J. Phys. Soc. Jpn. **55**, Suppl. (1986)], p. 61; H. Sakaguchi and M. Yosoi (private communication).

[11] H. O. Meyer, P. Schwandt, W. W. Jacobs, and J. R. Hall, Phys. Rev. C **27**, 459 (1983).

[12] J. R. Comfort, G. L. Moake, C. C. Foster, P. Schwandt, C. D. Goodman, J. Rapaport, and W. G. Love, Phys. Rev. C **24**, 1843 (1981).

[13] E. Stephenson, in *Antinucleon- and Nucleon-Nucleus Interactions,* edited by G. E. Walker, C. D. Goodman, and C. Olmer (Plenum, New York, 1985), p. 299.

[14] H. O. Meyer, P. Schwandt, H. P. Gubler, W. P. Lee, W. T. H. van Oers, R. Abegg, D. A. Hutchenson, C. A. Miller, R. Helmer, K. P. Jackson, C. Broude, and W. Bauhoff, Phys. Rev. C **31**, 1569 (1985).

[15] K. Jones, C. Glashausser, S. Nanda, R. de Swiniarski, T. Carey, W. Cornelius, J. McClelland, J. Moss, J.-L. Escudié, M. Franey, M. Gazzaly, N. Hintz, M. Haji-Saeid, G. Igo, C.Whitten, W. G. Love, and J. Comfort, in *Proceedings of the IX International Conference on High Energy Physics and Nuclear Structure, Versailles, 1981,* edited by P. Catillon, P. Radvanyi, and M. Proneuf (North-Holland, Amsterdam, 1982), p. 411.

[16] G. W. Hoffmann, M. L. Barlett, D. Ciskowski, G. Pauletta, M. Purcell, L. Ray, J. F. Amann, J. J. Jarmer, K. W. Jones, S. Penttilä, N. Tanaka, M. M. Gazzaly, J. R. Comfort, B. C. Clark, and S. Hama, Phys. Rev. C **41**, 1651 (1990).

[17] G. S. Blanpied, W. R. Coker, R. P. Liljestrand, G. W. Hoffmann, L. Ray, D. Madland, C. L. Morris, J. C. Pratt, J. E. Spencer, H. A. Thiessen, T. Kozlowski, N. M. Hintz, G. S. Kyle, M. A. Oothout, T. S. Bauer, G. Igo, R. J. Ridge, C. A. Whitten, Jr., P. M. Lang, H. Nann, and K. K. Seth, Phys. Rev. C **18**, 1436 (1978).

[18] G. S. Blanpied, G. W. Hoffmann, M. L. Barlett, J. A. McGill, S. J. Greene, L. Ray, O. B. Van Dyck, J. Amann, and H. A. Thiessen, Phys. Rev. C **23**, 2599 (1981).

[19] R. Bertini, R. Beurtey, F. Brochard, G. Bruge, H. Catz, A. Chaumeux, J. M. Durand, J. C. Faivre, J. M. Fontaine, D. Garreta, C. Gustafsson, D. Hendrie, F. Hibou, D. Legrand, J. Saudinos, and J. Thiron, Phys. Lett. **45B**, 119 (1973).

[20] G. D. Alkhazov, S. L. Belototsky, O. A. Domchenkov, Yu. V. Dotsenko, N. P. Kuropatkin, V. N. Nikulin, A. A. Vorobyov, and M. A. Shuvaev, Phys. Lett. **90B**, 364 (1980).

[21] J. M. Cameron, J. R. Richardson, W. T. H. van Oers, and J. W. Verba, Phys. Rev. **167**, 908 (1968).

[22] H. B. Eldridge, Ph. D. thesis, UCLA, 1967 (unpublished).

[23] H. B. Eldridge, S. N. Bunker, J. M. Cameron, J. R. Richardson, and W. T. H. van Oers, Phys. Rev. **167**, 915 (1968).

[24] H. Sakaguchi, M. Nakamura, K. Hatanaka, A. Goto, T. Noro, F. Ohtani, H. Sakamoto, H. Ogawa, and S. Kobayashi, Phys. Rev. C **26**, 944 (1982); H. Sakaguchi and M. Yosoi (private communication).

[25] H. Seifert, Ph. D. thesis, University of Maryland, 1990 (unpublished).

[26] J. Kelly, W. Bertozzi, T. N. Buti, F. W. Hersman, C. Hyde, M. V. Hynes, B. Norum, F. N. Rad, A. D. Bacher, G. T. Emery, C. C. Foster, W. P. Jones, D. W. Miller, B. L. Berman, W. G. Love, and F. Petrovich, Phys. Rev. Lett. **45**, 2012 (1980).

[27] J. Kelly, J. M. Finn, W. Bertozzi, T. N. Buti, F. W. Hersman, C. Hyde-Wright, M. V. Hynes, M. A. Kovash, B. Murdock, P. Ulmer, A. D. Bacher, G. T. Emery, C. C. Foster, W. P. Jones, D. W. Miller, and B. L. Berman, Phys. Rev. C **41**, 2504 (1990).

[28] J. J. Kelly, A. E. Feldman, B. S. Flanders, H. Seifert, D. Lopaino, B. Aas, A. Azizi, G. Igo, G. Weston, C. Whitten, A. Wong, M. V. Hynes, J. McClelland, W. Bertozzi, J. M. Finn, C. E. Hyde-Wright, R. W. Lourie, P. E. Ulmer, B. E. Norum, and B. L. Berman, Phys. Rev. C **43**, 1272 (1991).

[29] E. Blezynski, B. Aas, D. Adams, M. Bleszynski, G. J. Igo, T. Jaroszewicz, A. Ling, D. Lopiano, F. Sperisen, M. G. Moshi, C. A. Whitten, Jr., K. Jones, and J. B. McClelland, Phys. Rev. C **37**, 1527 (1988).

[30] B. S. Flanders, J. J. Kelly, H. Seifert, D. Lopiano, B. Aas, A. Azizi, G. Igo, G. Weston, C. Whitten, A. Wong, M. V. Hynes, J. McClelland, W. Bertozzi, J. M. Finn, C. E. Hyde-Wright, R. W. Lourie, B. E. Norum, and P. Ulmer, Phys. Rev. C **43**, 2103 (1991).

[31] G. S. Adams, Th. S. Bauer, G. Igo, G. Pauletta, C. A. Whitten, Jr., A. Wriekat, G. W. Hoffmann, G. Smith, M. Gazzaly, L. Ray, W. G. Love, and F. Petrovitch, Phys. Rev. Lett. **43**, 421 (1979).

[32] R. W. Fergerson, M. L. Barlett, G. W. Hoffmann, J. A. Marshall, E. C. Milner, G. Pauletta, L. Ray, J. F. Amann, K. W. Jones, J. B. McClelland, M. Gazzaly, and G. J. Igo, Phys. Rev. C **33**, 239 (1986).

[33] G. Bruge, Centre D'Etudes Nucléaires de Saclay Report No. Dph-N/ME/78-1, 1978 (unpublished).

[34] K. H. Bray, K. S. Jayaraman, G. A. Moss, W. T. H. van Oers, D. O. Wells, and Y. I. Wu, Nucl. Phys. **A167**, 57 (1971).

[35] E. T. Boschitz, R. W. Bercaw, and J. S. Vincent, Phys. Lett. **13**, 322 (1964).

[36] R. H. McCamis, T. N. Nasr, J. Birchall, N. E. Davison, W. T. H. van Oers, P. J. T. Verheijen, R. F. Carlson, A. J. Cox, B. C. Clark, E. D. Cooper, S. Hama, and R. L. Mercer, Phys. Rev. C **33**, 1624 (1986).

[37] R. M. Craig, J. C. Dore, G. W. Greenlees, J. S. Lilley, J. Lowe, and P. C. Rowe, Nucl. Phys. **58**, 515 (1964).

[38] E. E. Gross, R. H. Bassel, L. N. Blumberg, B. J. Morton, A. van der Woude, and A. Zucker, Nucl. Phys. **A102**, 673 (1967).

[39] L. N. Blumberg, E. E. Gross, A. van der Woude, A. Zucker, and R. H. Bassel, Phys. Rev. **147**, 812 (1966).

[40] R. M. Craig, J. C. Dore, J. Lowe, and D. L. Watson, Nucl. Phys. **86**, 113 (1966).

[41] H. Sakaguchi, M. Nakamura, K. Hatanaka, A. Goto, T. Noro, F. Ohtani, H. Sakamoto, H. Ogawa, and S. Kobayashi, Phys. Rev. C **26**, 944 (1982); H. Sakaguchi and M. Yosoi (private communication).

[42] P. Schwandt, H. O. Meyer, W. W. Jacobs, A. D. Bacher, S. E. Vigdor, M. D. Kaitchuck, and T. R. Donoghue, Phys. Rev. C **26**, 55 (1982).

[43] A. Nadasen, P. Schwandt, P. P. Singh, W. W. Jacobs, A. D. Bacher, P. T. Debevec, M. D. Kaitchuck, and J. T.

Meek, Phys. Rev. C **23**, 1023 (1981).

[44] J. Kelly, P. Boberg, A. E. Feldman, B. S. Flanders, M. A. Khandaker, S. D. Hyman, H. Seifert, P. Karen, B. E. Norum, P. Welch, S. Nanda, and A. Saha, Phys. Rev. C **44**, 2602 (1991).

[45] D. Frekers, S. S. M. Wong, R. E. Azuma, T. E. Drake, J. D. King, L. Buchmann, R. Schubank, R. Abegg, K. P. Jackson, C. A. Miller, S. Yen, W. A. Alford, R. L. Helmer, C. Broude, S. Mattsson, and E. Rost, Phys. Rev. C **35**, 2236 (1987).

[46] D. A. Hutcheon, J. M. Cameron, R. P. Liljestrand, P. Kitching, C. A. Miller, W. J. McDonald, D. M. Sheppard, W. C. Olsend, G. C. Neilson, H. S. Sherif, R. N. MacDonald, G. M. Stinson, D. K. McDaniels, J. R. Tinsley, L. W. Swensen, P. Schwandt, C. E. Stronach, and L. Ray, in *Proceedings of the Fifth International Symposium on Polarization Phenomena in Nuclear Physics, Santa Fe, 1980,* AIP Conf. Proc. No. 69, edited by G. C. Olsen, R. E. Brown, N. Jarmie, W. W. McNaughton, and G. M. Hale (AIP, New York, 1981), p. 454.

[47] G. W. Hoffmann, L. Ray, M. L. Barlett, R. Fergerson, J. McGill, E. C. Milner, K. K. Seth, D. Barlow, M. Bosko, S. Iverson, M. Kaletka, A. Saha, and D. Smith, Phys. Rev. Lett. **47**, 1436 (1981).

[48] A. Rahbar, B. Aas, E. Bleszynski, M. Bleszynski, M. Haji-Saeid, G. J. Igo, F. Irom, G. Pauletta, A. T. M. Wang, J. B. McClelland, J. F. Amann, T. A. Carey, W. D. Cornelius, M. Barlett, G. W. Hoffmann, C. Glashausser, S. Nanda, and M. M. Gazzaly, Phys. Rev. Lett. **47**, 1811 (1981).

[49] B. Aas, E. Bleszynski, M. Bleszynski, M. Haji-Saeid, G. Igo, F. Irom, G. Pauletta, A. Rahbar, A. Wang, J. F. Amann, T. A. Carey, W. Cornelius, J. B. McClelland, M. Barlett, G. Hoffmann, M. Gazzaly, C. Glashausser, and S. Nanda, Bull. Am. Phys. Soc. **26**, 1125 (1981).

[50] G. Igo, G. S. Adams, T. S. Bauer, G. Pauletta, C. A. Whitten, Jr., A. Wreikat, G. W. Hoffmann, G. S. Blanpied, W. R. Coker, C. Harvey, R. P. Lijestrand, L. Ray, J. E. Spencer, H. A. Thiessen, C. Glashausser, N. M. Huntz, M. A. Oothoudt, H. Nann, K. K. Seth, B. E. Wood, D. K. McDaniels, and M. Gazzaly, Phys. Lett. **81B**, 151 (1979).

[51] E. Bleszynski, M. Bleszynski, S. Hajisaeid, G. J. Igo, F. Irom, J. B. McClelland, G. Pauletta, A. Rahbar, A. T. M. Wang, C. A. Whitten, Jr., G. Adams, M. Barlett, G. W. Hoffmann, J. A. McGill, R. Boudrie, and G. Kyle, Phys. Rev. C **25**, 2563 (1982).

[52] R. W. Fergerson, M. L. Barlett, G. W. Hoffmann, J. A. Marshall, E. C. Milmer, G. Pauletta, L. Ray, J. F. Amann, K. W. Jones, J. B. McClelland, M. Gazzaly, and G. J. Igo, Phys. Rev. C **33**, 239 (1986).

[53] G. D. Alkhazov, T. Bauer, R. Beurtey, A. Boudard, G. Bruge, A. Chaumeaux, P. Couvert, G. Cvijanovich, H. H. Duhm, J. M. Fontaine, D. Garreta, A. Kulikov, D. Legrand, J. C. Lugol, J. Saudinos, J. Thirion, and A. A. Vorobyov, Nucl. Phys. **A274**, 443 (1976).

[54] J. B. Ball, C. B. Fulmer, and R. H. Bassel, Phys. Rev. **135**, B706 (1964).

[55] L. Ray, G. W. Hoffmann, G. S. Blanpied, W. R. Coker, and R. P. Liljestrand, Phys. Rev. C **18**, 1756 (1978).

[56] W. T. H. van Oers, H. Haw, and N. E. Davison, Phys. Rev. C **10**, 307 (1974).

[57] G. W. Hoffmann, L. Ray, M. Barlett, W. R. Coker, J. McGill, G. S. Adams, G. J. Igo, F. Irom, A. T. M. Wang, C.A. Whitten, Jr., R. L. Boudrie, J. F Amann, C. Glashausser, N. M. Hintz, G. S. Kyle, and G. S. Blanpied, Phys. Rev. C **24**, 541 (1981).

[58] B. C. Clark, S. Hama, and R. L. Mercer, in *Proceedings of the Workshop on the Interaction Between Medium Energy Nucleons in Nuclei* (Indiana University Cyclotron Facility, Bloomington, Indiana), AIP Conf. Proc. No. 97, edited by H. O. Meyer (AIP, New York, 1982), p. 260.

[59] B. C. Clark, in *Proceedings of the Workshop on Relativistic Dynamics and Quark-Nuclear Physics,* edited by M. B. Johnson and A. Picklesimer (Wiley, New York, 1986), p. 302.

[60] B. C. Clark, in *Proceedings of the International Symposium on Medium Energy Nucleon and Antinucleon Scattering, Bad Honnef, W. Germany,* edited by H. V. von Geramb (Springer, Berlin, 1985), p. 391.

[61] B. C. Clark, in *Proceedings of the Bates Users Theory Group Workshop on Relativistic Efects and Hadronic Structure, MIT (1985),* edited by J. Dubach and F. Gross (MIT, Cambridge, MA, 1985), p. 101.

[62] B. C. Clark, R. L. Mercer, and P. Schwandt, Phys. Lett. **122B**, 211 (1983).

[63] A. M. Kobos, E. D. Cooper, J. I. Johansson, and H. S. Sherif, Nucl. Phys. **A445**, 605 (1985).

[64] E. D. Cooper, S. Hama, B. C. Clark, and R. L. Mercer, AIP document no. PAPS PRVCA-47-297-88. Order by PAPS number and journal reference from the American Institute of Physics, Physics Auxiliary Publication Service, 335 E. 45th Street, New York, NY 10017.

[65] To obtain a copy of the FORTRAN program GLOBAL, please contact B. C. Clark, E. D. Cooper, or S. Hama at The Ohio State University. Bitnet address BCC@OHSTPY, COOPER@OHSTPY, or HAMA@OHSTPY. Files can be sent directly to those persons having E-MAIL addresses. The code is also available from anonymous FTP at pacific.mps.ohio-state.edu under the directory /tmp/global/.

[66] C. W. Glover, P. Schwandt, H. O. Meyer, W. W. Jacobs, J. R. Hall, A. D. Bacher, C. Olmer, M. Kaitchuck, and R. Devito, in IUCF Ann. Rep. 1 (1981).

[67] W. Bauhoff, At. Data Nucl. Data Tables **35**, 429 (1986).

[68] R. W. Finlay, in *Beijing International Symposium on Fast Neutron Physics, Beijing, PRC, 1991,* edited by S. M. Qain (Springer-Verlag, Berlin, 1992), p. 299.

[69] R. W. Finlay, G. Fink, W. Abfalter, P. Lisowski, G. L. Morgan, and R. C. Haight, in *International Conference on Nuclear Data for Science and Technology, Jülich, FRG, 1991,* edited by Sun Zuxung, Tang Hongqing, Xu Jincheng, and Zhang Jingshang (World Scientific, Singapore, 1992), p. 720.

[70] R. W. Finlay, G. Fink, W. Abfalter, P. Lisowski, G. L. Morgan, and R. C. Haight, Phys. Rev. C **46**, 237 (1992).

[71] R. Kozack and D. G. Madland, Phys. Rev. C **39**, 1461 (1989).

[72] R. Kozack and D. G. Madland, Nucl. Phys. **A509**, 664 (1990).

[73] R. L. Varner, W. J. Thompson, T. L. McAbee, E. J. Ludwig, and T. B. Clegg, Phys. Rep. **201**(2), 57 (1991).

[74] L. G. Arnold, B. C. Clark, R. L. Mercer, and P. Schwandt, Phys. Rev. C **23**, 1949 (1981).

[75] M. Jaminon, C. Mahaux, and P. Rochus, Phys. Rev. Lett. **43**, 1097 (1979).

[76] H. V. von Geramb, F. A. Brieva, and J. R. Rook, in *Microscopic Optical Potentials,* Lecture Notes in Physics Vol. 89, edited by H. V. von Geramb (Springer, Berlin, 1979),

p. 104.
[77] B. ter Haar and R. Malfliet, Phys. Rep. **149**, 207 (1987).
[78] B. C. Clark, S. Hama, R. L. Mercer, L. Ray, and B. D. Serot, Phys. Rev. Lett. **50**, 1644 (1983).
[79] D. P. Murdock and C. J. Horowitz, Phys. Rev. C **35**, 1442 (1987).
[80] N. Ottenstein, S. J. Wallace, and J. A. Tjon, Phys. Rev. C **38**, 2272 (1988).
[81] S. Hama, B. C. Clark, R. E. Kozack, S. Shim, E. D. Cooper, R. L. Mercer, and B. D. Serot, Phys. Rev. C **37**, 1111 (1988).
[82] B. D. Serot and J. D. Walecka, in *Advances in Nuclear Physics, Vol. 16,* edited by J. W. Negele and E. Vogt (Plenum, New York, 1986).
[83] H. A. Bethe, Phys. Rev. **57**, 1125 (1940).
[84] V. R. Pandharipande and S. C. Pieper, Phys. Rev. C **45**, 791 (1992).
[85] J. W. Negele and K. Yazaki, Phys. Rev. Lett. **47**, 71 (1981).
[86] T. Cheon, Phys. Rev. C **38**, 1516 (1988).
[87] P. V. Renberg, D. F. Measday, M. Pepin, P. Schwaller, B. Favier, and C. Richard-Serre, Nucl. Phys. **A183**, 81 (1972).
[88] H. O. Meyer and P. Schwandt, Phys. Lett. **107B**, 353 (1981).
[89] B. C. Clark, E. D. Cooper, S. Hama, R. W. Finlay, and T. Adami, Phys. Lett. (in press).
[90] M. Jaminon and C. Mahaux, Phys. Rev. C **40**, 354 (1989).